JCTC Journal of Chemical Theory and Computation

pubs.acs.org/JCTC Article

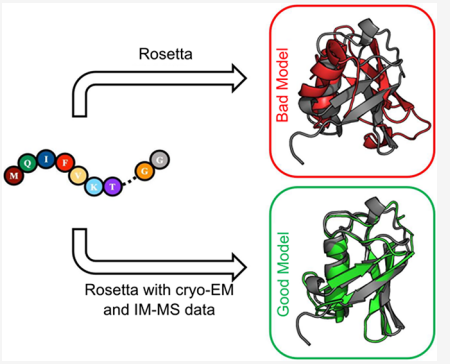
Improving Protein Structure Prediction Using Integrative Cryo-EM and Ion Mobility Mass Spectrometry Modeling

Jacob B. Howard,[§] Akshaya Narayanasamy,[§] and Steffen Lindert*

Cite This: J. Chem. Theory Comput. 2026, 22, 5909−5917 Read Online

ACCESS | Metrics & More | Article Recommendations | Supporting Information

ABSTRACT: Proteins play essential roles in cellular processes, and accurate three-dimensional structures are critical for understanding function and enabling drug discovery. High-resolution methods such as cryo-electron microscopy (cryo-EM) and X-ray crystallography can provide detailed structural information. However, many proteins are characterized only by low-resolution or sparse data, which are difficult to translate into accurate atomic models. Mass spectrometry-based approaches such as ion mobility (IM-MS) provide global structural information through collisional cross section (CCS) but lack atomistic detail. Here, we present CRIM (cryo-EM + IM-MS), an integrative Rosetta scoring function that combines low-resolution cryo-EM density with IM-MS-derived CCS restraints to improve monomeric protein structure prediction. CRIM integrates the REF2015 energy with CCS agreement (via PARCS) and an electron density term (elec_dens_fast). On an ideal data set of 60 proteins, CRIM reduced the mean RMSD from 3.65 to 2.90 Å and increased the TM-score from 0.88 to 0.90. On an experimental data set of 54 proteins, CRIM improved model selection, lowering the RMSD from 6.65 to 4.38 Å and increasing the TM-score from 0.73 to 0.79. Compared to AlphaFold3, CRIM produced competitive predictions and outperformed it for select challenging targets where sparse experimental data provide strong constraints. The CRIM score function is freely available within Rosetta and provides a practical framework for integrating complementary cryo-EM and IM-MS data to improve protein structure prediction.



Downloaded via UNIV OF CALIFORNIA LOS ANGELES on July 8, 2026 at 17:53:18 (UTC).
See https://pubs.acs.org/sharingguidelines for options on how to legitimately share published articles.

INTRODUCTION

Proteins are fundamental for most cellular processes, and understanding their three-dimensional structure is crucial for elucidating function and applications in drug discovery,[1,2] vaccine design,[3] and other biotechnological applications.[4] High-resolution techniques such as X-ray crystallography, nuclear magnetic resonance (NMR) spectroscopy, and cryo-electron microscopy (cryo-EM) are instrumental in determining protein structures at atomic resolutions.[5] Occasionally, however, some of these higher resolution techniques only yield structural information at lower resolutions, such as when lower-resolution density maps are obtained from cryo-EM, or when NMR experiments yield sparse data.[6−10]

In addition to high-resolution approaches, a variety of experimental techniques provide sparse, yet valuable structural information. Mass spectrometry (MS) is a prominent example, offering rapid data collection, minimal sample requirements, and broad applicability across a wide range of protein sizes and heterogeneous samples. Several MS-based methods are routinely employed to probe structural features, including hydrogen/deuterium exchange (HDX), chemical cross-linking (XL-MS),[11] surface-induced dissociation (SID),[12] covalent labeling (CL), and ion mobility (IM-MS).[13,14] IM-MS provides a collisional cross section (CCS) value, which reflects the overall size and shape of an ion based on a rotationally averaged cross-sectional area, thereby enabling characterization of conformational states. Although the structural information from these lower-resolution methods is insufficient to resolve atomic coordinates, it nonetheless offers critical constraints that may complement those of high-resolution or computational techniques.

In parallel, recent advances in machine learning, particularly with deep learning models like AlphaFold3 (AF3),[15] Boltz2,[16] and RosettaFold2,[17] have significantly enhanced our ability to predict protein structures computationally. While these models are highly effective and frequently yield accurate predictions, there is a significant number of proteins that remain challenging to predict.[18] To improve computational structure prediction, integrating sparse experimental data into the prediction process can further improve the accuracy of these predictions.[19]

Previous studies have demonstrated that diverse experimental data types can be incorporated into modeling frameworks such as Rosetta to improve protein structure predictions.[20−22] For example, XL-MS data have been used as upper-bound distance

Received: February 11, 2026
Revised: May 5, 2026
Accepted: May 7, 2026
Published: May 14, 2026



© 2026 American Chemical Society

https://doi.org/10.1021/acs.jctc.6c00265
J. Chem. Theory Comput. 2026, 22, 5909−5917

restraints,[23,24] and CL experiments provided complementary constraints that refine surface exposure and topology in modeled structures.[25−29] SID measurements provided guidance on subunit connectivity and noncovalent interaction energetics,[30−34] and IM-MS experiments provided collisional cross section (CCS) values that describe overall molecular shape and size enabling discrimination between candidate structures.[14,35−41] Beyond mass spectrometry, low-resolution cryo-EM density maps can be directly integrated into modeling protocols, supplying spatial localization constraints that further refine structural predictions.[9,10,23,32,42−44] Furthermore, integrative approaches that combine multiple complementary experimental techniques have also been shown to be successful. Seffernick et al. demonstrated that integrating SID mass spectrometry data with cryo-EM maps improved the accuracy of protein complex modeling beyond what was observed when just SID or cryo-EM was used independently.[32] Similarly, studies combining ion mobility with chemical cross-linking have successfully refined modeling of large protein assemblies by simultaneously constraining both overall shape and specific residue−residue distances.[45] These examples illustrate how incorporating diverse experimental data sets into computational modeling frameworks can yield more robust and biologically meaningful structural predictions.[46]

In this study, we extend these integrative approaches to the problem of monomeric protein structure prediction. We present the CRIM (cryo-EM + IM-MS) score function, which incorporates sparse data obtained from low-resolution (>6 Å) cryo-EM density maps and IM-MS in the form of CCS values into Rosetta comparative modeling (CM) to improve protein structure predictions. With our method, we were able to improve structure predictions across 83% of the monomeric proteins in both our data sets from an average RMSD of 5.1 Å with the Rosetta REF2015 (RS) score function to 3.6 Å RMSD with the new CRIM score function. The CRIM score function is part of the Rosetta software suite and is freely available for access by the users (GitHub link: https://github.com/RosettaCommons/rosetta/).

METHODS

Ideal Data Set Construction

To evaluate the performance of the CRIM scoring function for idealized, noise- and error-free data, we used a previously assembled ideal data set of 60 monomeric proteins.[40] Structures in the ideal data set represent all unique protein architecture categories as classified by the CATH Protein Structure Classification Database, with sequence lengths ranging from 58 to 965 amino acids. For each protein, synthetic experimental data was generated: collision cross section (CCS) values were calculated using the Rosetta PARCS algorithm,[40,47] and low-resolution cryo-electron microscopy (cryo-EM) density maps were simulated using the BCL density module as described below.

Structural models for each of the 60 proteins in ideal data set were generated using Rosetta multitemplate Comparative Modeling (CM).[48] Following established protocols, 10,000 models were produced for each protein.[40] The 3mer and 9mer fragment libraries were created using the Rosetta fragment picker tool.[49] BLAST was used to identify both low and high sequence similarity templates, which were included to broaden the diversity of the model set. Additionally, template weights were varied to produce both native-like (<5 Å RMSD) and non-native-like (>5 Å RMSD) models compared to the target protein. All structures generated with RosettaCM were subject to the Rosetta fast relax protocol prior to scoring.

Models were scored using the RS score function[50] and the CRIM function, respectively, to assess their ability to distinguish native-like and non-native-like conformations. Model quality was evaluated using α-carbon root-mean-square deviation (Cα-RMSD) calculated in PyMOL, and TM-score values were computed with TM-align.[51]

Benchmark Data Set Construction

To evaluate CRIM under relevant experimental conditions, we curated a benchmark data set of 54 monomeric proteins. Of these, 30 of the target proteins had experimentally determined cryo-EM density maps and 24 had published IM-MS CCS measurements. Detailed source information on the experimental measurements of IM-MS CCS data is found in the Supporting Information. Among these 54 proteins, 2 of them had both experimental cryo-EM density map and IM-MS CCS measurements. To enable integrated scoring across the full benchmark set, the missing data for each target was simulated: density maps were generated with BCL for targets with CCS data only, and CCS values were computed with PARCS for targets with cryo-EM data only. For each benchmark protein, 10,000 models were generated using the same RosettaCM protocol applied to the ideal data set.

Low-Resolution Cryo-EM Density Map Preparation

Within the benchmark data set, 30 proteins had experimental cryo-EM density maps. However, the density maps were often for entire complexes, which would affect the scoring process of monomeric proteins when using the "elec_dens_fast" score term. As a solution, the density maps were cropped within 5 Å of the native structure using ChimeraX.[52]

For the remaining targets in the benchmark data set, along with all the proteins in the Ideal data set, the density maps were simulated using the BCL density package. All density maps were simulated from crystal structures using BCL:density:FromPDB[53] at 14 Å resolution, with a voxel size of 1.4 Å and a Gaussian noise level set to 0.8.

Native CCS Calculations for Proteins without IM-MS Data

Theoretical CCS values were computed from atomic coordinates using the Rosetta PARCS algorithm.[40] Each structure was randomly rotated 300 times to obtain a rotationally averaged CCS. CCS calculations were performed with the buffer-gas radius set to 1.0 Å to approximate helium-based ion mobility conditions. Helium CCS values are widely used as a standard reference in ion mobility studies and are commonly employed for calibration and comparison with theoretical models due to their extensive availability in the literature.[54]

CCS values had to be calculated from the native structure for all 60 proteins in the ideal data set and 30 proteins in the benchmark data set. Several of these native proteins had missing residues within their PDB structures. Because PARCS calculates CCS values based on the atoms present in a PDB file, missing residues in the structure may result in an underestimation of the native CCS values. For native structures with missing residues in their PDB entries, a modified RosettaCM pipeline was employed to reconstruct the full sequence across both data sets. For this RosettaCM protocol, only templates with high sequence similarity were utilized, in addition to the crystal structure with the missing residues. Furthermore, the crystal structure was weighted more highly than the other templates so that near-native-like predictions could be obtained. With this protocol, only 250 structures were predicted for each protein system. The best-scoring model generated from this pipeline for each target protein was used to compute the theoretical CCS value by using PARCS. We used this CCS value as the benchmark against the models in place of the experimental IM-MS data.

Protein Structure Prediction with AlphaFold3

For each protein in the ideal and benchmark data sets, structures were generated using AlphaFold3 v3.0.1 on the Cardinal cluster at the Ohio Supercomputer Center. Predictions were made by using the standard AF3 settings. The highest-ranked AF3 model for each protein was used in comparison to the best-scoring CRIM predicted models.

CRIM Score Function

Density maps and CCS values from cryo-EM and IM-MS experiments, respectively, were incorporated into the RS score function to act as spatial restraints for integrative Rosetta modeling. The Cryo-EM and IM score terms provide information regarding a protein's overall shape, size, and spatial density. To integrate this information into Rosetta, the $IM_{Score\ Term}$ was adapted from a previously implemented score term to

https://doi.org/10.1021/acs.jctc.6c00265
J. Chem. Theory Comput. 2026, 22, 5909−5917

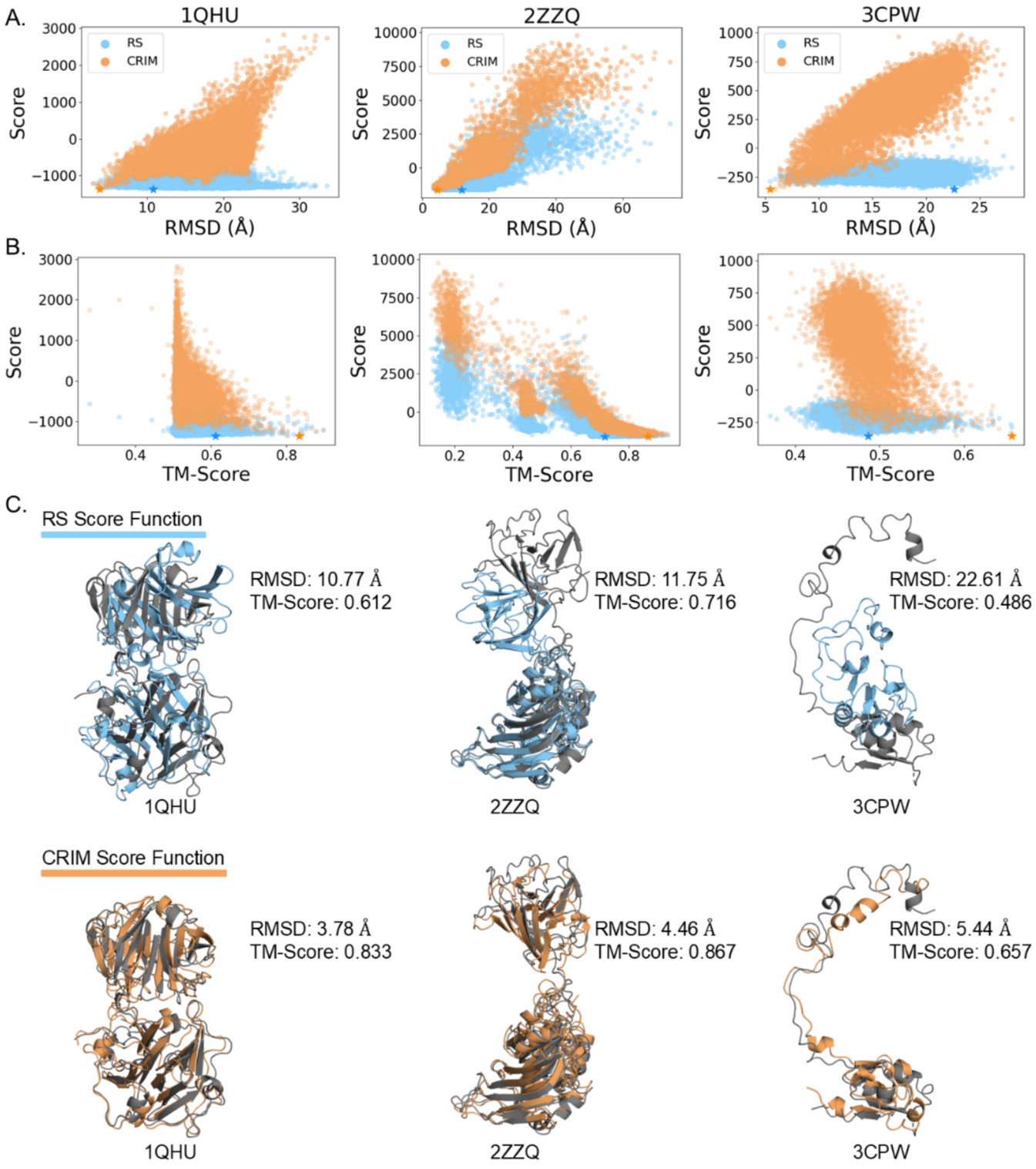


Figure 1. (A) Score vs RMSD distributions for the 10,000 model structures of proteins 1QHU, 2ZZQ, and 3CPW when scored with the CRIM score function (orange) compared to the RS score function (light blue). For both score functions, the best-scoring structure is indicated with a star in its respective color. The score values for the CRIM score function were normalized to the RS scores by subtracting the difference between the two best-scoring structures from all 10,000 of the model scores. (B) The corresponding score vs TM-score distributions of the models scored with the CRIM score function (orange) compared to the RS score function (light blue). (C) Predicted models for the three proteins using the RS score function (light blue) versus the CRIM score function (orange), each overlaid with the native structures (gray).

quantify the agreement of a predicted model with the IM-MS data.[40] The $IM_{Score\ Term}$ is a piecewise penalty function (defined in eq 1) based on the difference (ΔCCS) between CCS_{PARCS} and CCS_{IM}. The function uses a lower bound (LB) to account for error and an upper bound (UB) to cap the penalty for large deviations (shown in eq 1). ΔCCS values below the LB (25 $Å^2$) do not receive a penalty, and ΔCCS above the UB (125 $Å^2$) receive the maximum penalty of 125, with a fade function used in between.

https://doi.org/10.1021/acs.jctc.6c00265
J. Chem. Theory Comput. 2026, 22, 5909−5917

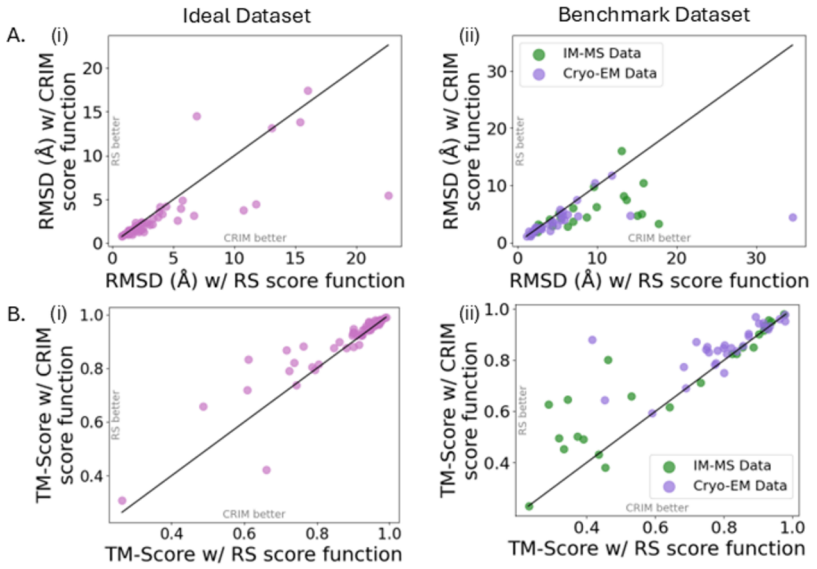


Figure 2. Evaluation of structural accuracy using CRIM versus RS score functions. (A) RMSD of the top-ranked models, presented for the ideal data set (i) and the benchmark data set (ii) separated by proteins with IM-MS data (green) and cryo-EM data (purple). (B) TM scores of the highest-ranking models, reported for the ideal data set (i) and the benchmark data set (ii) separated by proteins with IM-MS data (green) and cryo-EM data (purple).

$$\mathrm{IM}_{\mathrm{Score\ Term}} = \begin{cases} 0 & \text{if } \Delta\mathrm{CCS} < \mathrm{LB} \\ 100(2x^3 - 3x^2 + 1) & \text{if } \mathrm{LB} < \Delta\mathrm{CCS} < \mathrm{UB} \\ 125 & \text{if } \Delta\mathrm{CCS} > \mathrm{UB} \end{cases}$$
$$x = -\left(\frac{\Delta\mathrm{CCS} - \mathrm{UB}}{\mathrm{UB} - \mathrm{LB}}\right) \quad (1)$$

The cryo-$\mathrm{EM}_{\mathrm{Score\ Term}}$ is a previously implemented score term in Rosetta (elec_dens_fast) and was calculated based on model agreement with either experimental cryo-EM density maps or the simulated density maps.[55] The evaluation score, $\mathrm{CRIM}_{\mathrm{Score}}$, was defined as a weighted sum of the RS score function, $\mathrm{IM}_{\mathrm{Score\ Term}}$, and cryo-$\mathrm{EM}_{\mathrm{Score\ Term}}$ as shown in eq 2.

$$\mathrm{CRIM}_{\mathrm{Score}} = \mathrm{RS} + 2(\mathrm{IM}_{\mathrm{Score\ Term}}) + 10(\text{cryo-}\mathrm{EM}_{\mathrm{Score\ Term}}) \quad (2)$$

The total CRIM score captures both structural conformity to the standard Rosetta score and quantitative agreement with sparse experimental data from cryo-EM and IM-MS. This integrated scoring strategy was hypothesized to improve the selection of near-native structures across data sets with diverse experimental resolutions and data completeness.

RESULTS AND DISCUSSION

CRIM Score Function Improved Model Selection in an Ideal Data Set

In this study, we hypothesized that integrating cryo-EM density information with IM-MS data would provide complementary constraints. This integration would enable more accurate monomeric protein structure prediction than can be achieved with either method alone. As both cryo-EM and IM-MS are becoming more accessible and widely used, it is increasingly likely in the future that both data types will be available for the same protein target, underscoring the need for computational methods capable of leveraging these data sets together. To test this hypothesis, we assessed the performance of the CRIM score function using an ideal data set of 60 monomeric proteins, designed to represent diverse protein folds across the CATH classification. In this data set, synthetic experimental data was generated by simulating CCS values with the Rosetta PARCS algorithm[40] and cryo-EM density maps with the BCL density package.[10,53] For each protein, 10 000 model structures were generated with Rosetta comparative modeling (RosettaCM), and all models were subsequently rescored using the CRIM function to evaluate its ability to discriminate between native-like and non-native conformations.

For both scoring functions, the lowest-scoring model was considered the best or predicted structure. Upon incorporating cryo-EM and IM-MS data through the CRIM score function, we found a notable improvement in the accuracy of the best-scoring models compared to predictions made using only the RS score function. The structures predicted by CRIM exhibited an average RMSD of 2.90 Å, compared to 3.65 Å with the RS score function. The average TM scores also improved, increasing from 0.88 with RS to 0.90 with CRIM. Three proteins demonstrating significant improvement in RMSD with the CRIM score function are illustrated in Figure 1. Figure 1A,B shows that incorporating experimental data not only resulted in more accurate structural predictions but also penalized inaccurate conformations more strongly, yielding significantly more clearly defined energy funnels across the proteins. As illustrated in Figure 1C, the CRIM score function guided model selection toward native-like conformations for all three proteins. For example, hemopexin (PDB ID: 1QHU) improved from 10.77 Å RMSD with RS to 3.78 Å with CRIM, while pORF2 (PDB ID: 2ZZQ) improved from 11.75 to 4.46 Å. Even for the 50S ribosomal protein L15 (PDB ID: 3CPW), which was one of the most challenging proteins in the ideal data set, the CRIM score function reduced the RMSD from 22.61 to 5.44 Å, indicating that substantial gains can be achieved across diverse structural contexts. Similar results were observed for the other proteins in the ideal data set, as shown in Figures S1−S3.

Across the ideal data set, the RMSD of the predicted structures either improved or remained the same for 50 out of the 60 proteins, with an average improvement of 1.44 Å among the proteins that saw an improvement (Figure 2A(i)). Likewise, the TM-score improved for 49 out of 60 proteins with an average improvement of 0.04 over the RS score function for those

https://doi.org/10.1021/acs.jctc.6c00265
J. Chem. Theory Comput. 2026, 22, 5909−5917

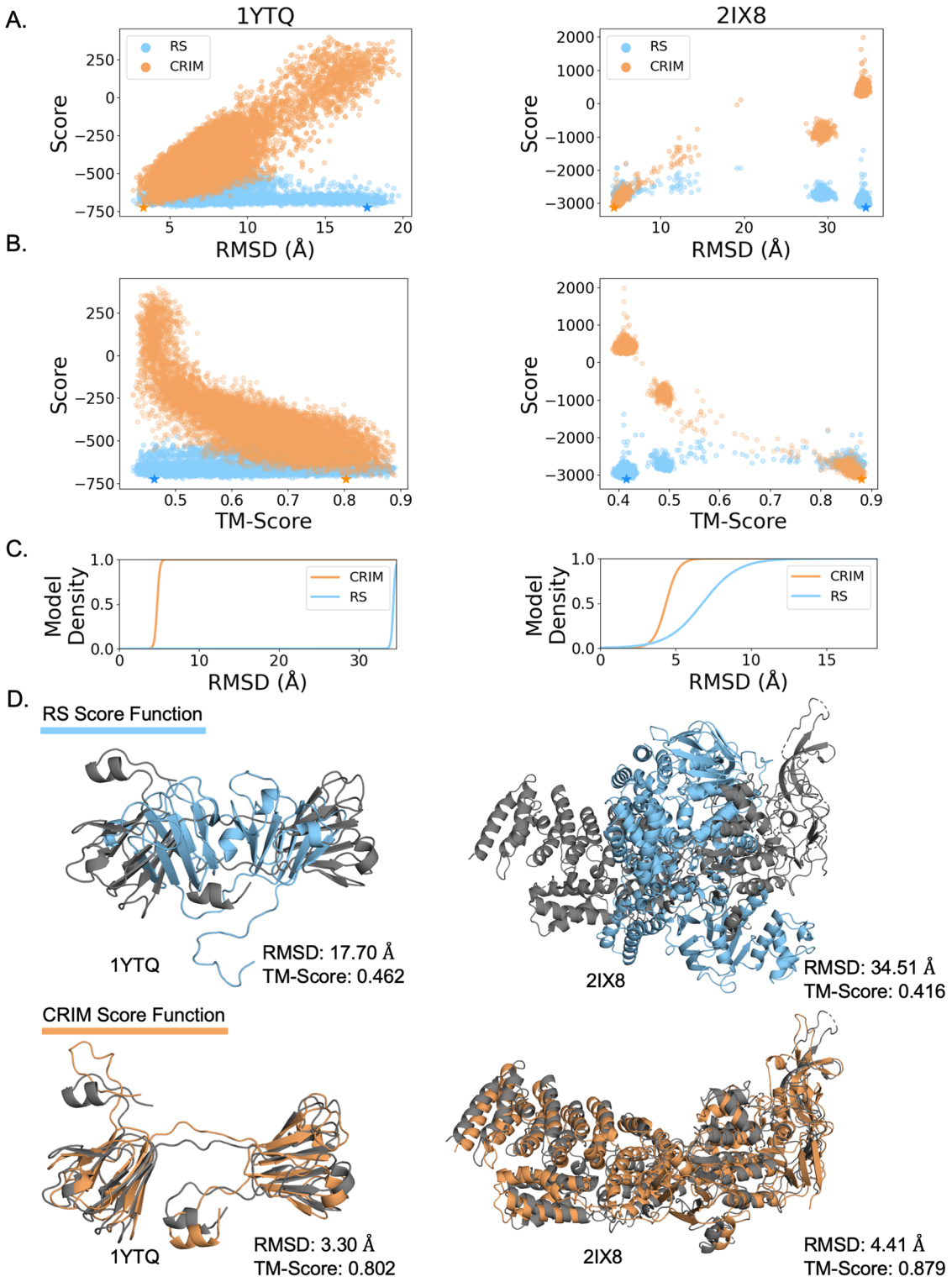


Figure 3. (A) Score versus RMSD distributions for the 10,000 model structures of 1YTQ and 2IX8 using the CRIM score function (orange) and the RS score function (light blue). For both score functions, the best-scoring structure is indicated with a star in its respective color. (B) TM-score vs RMSD distributions of the models scored with the CRIM score function compared to the RS score function. (C) Cumulative density plots for the RMSD of top 100 scoring models. (D) The predicted models using the CRIM score function (orange) compared to the models predicted with the RS score function (light blue) with each of the models overlaid on the native structure (gray).

proteins (Figure 2B(i)). Visually, most points lie below (RMSD) or above (TM-score) the $x = y$ line, suggesting an improved prediction, and the deviation from the line grows at higher RS RMSD values, indicating stronger benefits for harder targets. These results further support that the addition of simulated cryo-EM and IM-MS data refines the ability of the RS score function to distinguish between native and non-native-like models. However, since the simulated, idealized data is not identical to real experimental data, we further tested the

https://doi.org/10.1021/acs.jctc.6c00265
J. Chem. Theory Comput. 2026, 22, 5909−5917

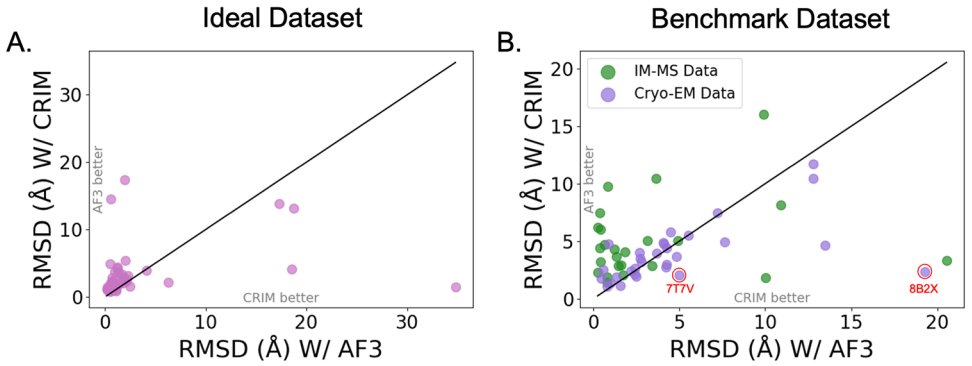


Figure 4. Comparison of structural accuracy when using the CRIM score function versus AF3. (A) RMSD of the top-ranked models for the ideal data set. (B) RMSD of the top-ranked models for the benchmark data set separated by proteins with IM-MS data (green) and cryo-EM data (purple). The two circled and labeled data points indicate the protein structures that were deposited in the PDB after the AF3 training date cutoff.

effectiveness of the CRIM score function in conjunction with experimental data.

Cryo-EM and IM-MS Data Improved Model Selection in the Experimental Data Set

The experimental data set consisted of 52 proteins with either experimental data from cryo-EM or IM-MS and two proteins that have both experimental data types. The data were curated as described in the Methods section. For each protein in the experimental data set, 10,000 models were generated with Rosetta Comparative Modeling and were rescored with the cryo-EM and IM-MS data.

Again, we saw an improvement in model selection quality with the addition of the CRIM score function as compared to the RS score function (Figure 2A(ii),B(ii)). The average best-model RMSD dropped from 6.65 Å (RS) to 4.38 Å (CRIM), and the mean TM-score rose from 0.73 (RS) to 0.79 (CRIM). Notably, most proteins benefited: 46/54 showed equal or lower RMSD with CRIM (Figures 2A(ii) and S4), and 43/54 showed equal or higher TM scores (Figures 2B(ii) and S5). For the 46 proteins with lower RMSD values, we observed an average improvement of 3.40 Å (corresponding to an improvement of 0.09 in TM-score), with 20 of those achieving a greater than 1 Å RMSD reduction, and 17 achieving a greater than 0.05 TM-score increase, indicating widespread practical improvement with the CRIM score function. For the two proteins with both experimental data types, we observed improvements in model selection. The proteins lysozyme and insulin (PDB ID: 1DPX and 3INS) saw an average improvement from 5.95 Å to 4.02 Å RMSD and an average change in TM-score from 0.49 to 0.52, using the RS and CRIM score functions, respectively (see Figure S6). These results further demonstrate that model selection with experimental cryo-EM and IM-MS data outperformed that of just the RS score function.

Furthermore, Figure 3 highlights two benchmark proteins, βB2-Crystallin (PDB ID: 1YTQ) and eEF3 (PDB ID: 2IX8), where the CRIM score function significantly improved predictions over the RS score function. Figure 3A shows the RMSD vs score distributions of the models when scoring with the CRIM score function (orange) compared to scoring with the RS score function (blue). The corresponding TM-score distributions are shown in Figure 3B. We used an experimental CCS value for 1YTQ, whereas the cryo-EM density map was simulated as described in the Methods section. 2IX8 had an experimental low-resolution cryo-EM density map, and the CCS value was simulated with PARCS. In both cases, we saw significantly better models selected when using the CRIM score function. Notably, both RS predictions had a TM-score below 0.5, which indicates that the predicted model did not share a similar fold to the native structure. However, when experimental data was included and the models were rescored with the CRIM score function, both predicted models exhibited a TM-score over 0.8, which indicates a highly similar structure between the predicted model and the native structure. This further supports that integrating these two types of experimental data does help in predicting the structures of monomeric proteins.

We performed a cumulative density plot analysis to understand if there was improvement in the 100 top-scoring models' RMSD as depicted in Figure 3C. For the two example proteins, the CRIM score function significantly shifted the distribution of the top 100 scoring models toward a lower RMSD value than when the RS score function was used. In both cases, the CRIM score function achieved a near-complete density saturation at around 6 Å RMSD, whereas density saturation for models scored with the RS score function was only observed for RMSD values beyond 10 Å in both cases. This trend was seen throughout the experimental data set (Figure S7), showing that the CRIM score function consistently scored models more accurately than the RS score function (even in cases where the top-scoring model did not improve significantly).

CRIM Score Term Analysis

To evaluate how each experimental data type contributed to the rescoring of protein models, we analyzed the IM-MS and cryo-EM score terms individually and in combination. Because density maps are far more information-rich than a single CCS value, the cryo-EM term contributed the majority of the total prediction improvement for most models. The IM-MS term, however, proved essential for achieving the best results across both the experimental and ideal data sets (see Figure S8). CRIM outperformed the cryo-EM term alone for 94 of 114 proteins, and 10 of those 94 improved solely due to the IM-MS contribution, showing no improvement, and in some cases performing worse when rescored with cryo-EM data alone. Particularly, we observed cases such as antigen protein (PDB ID: 4H2A) and CAS1 protein (PDB ID: 4XTK) where improvements were only achieved when both cryo-EM and ion mobility data were used together, as well as instances where ion mobility contributed to improved model selection in situations where cryo-EM alone was insufficient (see Figure S9). These results emphasize the complementary nature of the two data sources and support the value of integrating both into a unified scoring framework.

https://doi.org/10.1021/acs.jctc.6c00265
J. Chem. Theory Comput. 2026, 22, 5909−5917

Structure Prediction Using CRIM Is Competitive with AF3

AF3 is the state-of-the-art technique for protein structure prediction.[15] Thus, we compared the best CRIM predictions for the proteins in both the ideal and benchmark data set to the respective AF3 predictions to contextualize the benefit of incorporating sparse experimental data into protein structure prediction (see Figure S10 for the full RMSD distributions across AF3, RS, and CRIM). For the ideal data set (Figure 4A), the mean RMSD for the AF3 predictions was 2.55 Å, compared to a mean RMSD of 2.90 Å with the CRIM score function. While on average, AF3 slightly outperformed CRIM, 36/60 (60%) of the predictions were within 1.0 Å of each other, and for additional 5 proteins, CRIM outperformed AF3 by more than 1 Å RMSD. Thus, CRIM performed similarly or better than AF3 for 41/60 (68%) of the structures predicted, as shown in Figure 4A. Similar trends were seen for the benchmark data set comparison (Figure 4B). The mean RMSD for the AF3 predictions was 4.12 Å compared to 4.38 Å when using the CRIM score function. Across the data set, 20/54 (37%) of the predictions were within 1 Å of each other, and for 12/54 proteins, CRIM produced lower RMSD models than AF3 by more than 1 Å RMSD. Notably, based on AF3's reported training cutoff date of 09/30/2021, all proteins in the ideal data set and all but two proteins in the benchmark data set were potentially included in AF3 training; the two benchmark proteins deposited after this cutoff (8B2X and 7T7V) were both predicted substantially better by CRIM (RMSD values of 2.3 and 2.0 Å, respectively) than by AF3 (RMSD values of 19.3 Å and 5.0 Å, respectively). Collectively, these results demonstrate that although AF3 remains the more accurate method on average, CRIM frequently produced predictions that are competitive with AF3 and can substantially outperform AF3 for select targets when sparse experimental restraints provide strong discriminatory power. This observation is consistent with the broader motivation for CRIM. Experimentally grounded restraints reduce ambiguity and improve discrimination between native-like and non-native-like conformations, thereby improving predictions for difficult targets. Looking forward, an important extension of this work will be to incorporate sparse experimental information directly into machine learning-based structure prediction workflows such as AF3, for example, by using IM-MS and cryo-EM-derived restraints during model generation and/or as part of a restraint-guided refinement stage. Integrating these orthogonal experimental constraints into machine learning pipelines could further reduce the frequency of inaccurate predictions and improve reliability for difficult targets, extending the benefits of sparse experimental data to next-generation structure prediction workflows.

CONCLUSION

This study introduced the Rosetta CRIM score function, an integrative scoring strategy that augments the RS score function with sparse cryo-EM density and IM-MS information to guide monomeric protein structure selection. Across an idealized, noise-free data set of 60 proteins, CRIM consistently identified more native-like structures relative to RS alone, lowering the average best-model RMSD from 3.65 to 2.90 Å and increasing the mean TM-score from 0.88 to 0.90. In an experimental data set of 54 proteins with either experimental cryo-EM or IM-MS data (and the complementary modality simulated), CRIM again improved quality: the mean best-model RMSD decreased from 6.65 to 4.38 Å and the mean TM-score rose from 0.73 to 0.79. The improvement was most pronounced for harder targets, where the additional information provided by IM-MS (shape information from CCS) and cryo-EM density helped to more clearly distinguish between native-like and non-native-like models. This clearly demonstrates the utility of integrative IM-MS/cryo-EM modeling for both ideal and experimental data sets. The CRIM score function is freely available as part of the Rosetta software suite. A detailed tutorial of the protein structure scoring pipeline is provided in the Supporting Information.

Moving forward, we plan to extend the CRIM score function beyond monomeric targets as predicting complexes is a limitation of this method to explicitly handle protein complexes, where constraints from CCS and cryo-EM density can be integrated to improve discrimination among predicted architectures. Furthermore, incorporating CRIM into next-generation deep learning tools such as AlphaFold is an additional, natural extension of this work. AlphaFold frequently achieves high accuracy; however, it faces limitations for larger proteins, when evolutionary signals are weak, or for proteins with disordered regions and/or multiple conformations.[56,57] In these settings, CRIM's constraints from IM-MS data and low-resolution cryo-EM maps may add experimentally grounded information that helps reduce ambiguity and improve reliability for more difficult targets.

Finally, because CRIM combines IM-MS and electron microscopy information in a single framework, it may also be useful for modeling soft-landed proteins. Soft-landing workflows naturally pair native MS/IM-MS measurements with electron microscopy on the deposited sample,[58−60] which matches well with the types of data CRIM is designed to use. In this context, CRIM could help evaluate whether soft-landed proteins remain native-like and help select or refine structural models that agree with both the measured CCS value and the resulting EM density.

ASSOCIATED CONTENT

Supporting Information

The Supporting Information is available free of charge at https://pubs.acs.org/doi/10.1021/acs.jctc.6c00265.

Score versus RMSD (Figures S1 and S4, Analysis of proteins that had both experimental cryo-EM and IM-MS CCS data (Figures S6); score versus TM-score (Figures S2 and S5); cumulative density plots (Figures S3 and S7); comparison of the average RMSDs (Figures S8 and S10); comparison of the best-scoring structures (Figure S9); and a tutorial for using the CRIM score function (PDF)

PDB ID, protein name, sequence length, experimental CCS value, experiment type, charge state, buffer gas, simulated CCS value (using PARCS), and the corresponding publication sources of the IM-MS CCS values used in this manuscript (XLSX)

AUTHOR INFORMATION

Corresponding Author

Steffen Lindert − *Department of Chemistry and Biochemistry, University of California, Los Angeles, Los Angeles, California 90095, United States;* orcid.org/0000-0002-3976-3473; Email: lindert@ucla.edu

Authors

Jacob B. Howard − *Department of Chemistry and Biochemistry, Ohio State University, Columbus, Ohio 43210, United States*

https://doi.org/10.1021/acs.jctc.6c00265
J. Chem. Theory Comput. 2026, 22, 5909−5917

Akshaya Narayanasamy − *Department of Chemistry and Biochemistry, University of California, Los Angeles, Los Angeles, California 90095, United States*

Complete contact information is available at: https://pubs.acs.org/10.1021/acs.jctc.6c00265

Author Contributions

[§]J.B.H. and A.N. contributed equally.

Notes

The authors declare no competing financial interest.

■ ACKNOWLEDGMENTS

We thank fellow Lindert lab members for their valuable discussions and guidance. We also acknowledge the computational resources provided by the Ohio Supercomputer Center (OSC).[61] We are grateful to the Rosetta Commons community for developing and maintaining the Rosetta software suite and for making these tools broadly available. We thank Dr. S. M. Bargeen Alam Turzo for his work on developing PARCS. This work was supported by NIH (RM1-GM149374 to S.L.). We additionally acknowledge support from the NSF RaMP (Research and Mentoring for Postbacs; NSF 2216011 to S.L.) program for training, mentorship, and community resources that contributed to this work.

■ REFERENCES

(1) Coelho, E. D.; Arrais, J. P.; Oliveira, J. L. From protein-protein interactions to rational drug design: are computational methods up to the challenge? *Curr. Top Med. Chem.* **2013**, *13* (5), 602−618.
(2) Leelananda, S. P.; Lindert, S. Computational methods in drug discovery. *Beilstein J. Org. Chem.* **2016**, *12*, 2694−2718.
(3) Huang, P. S.; Boyken, S. E.; Baker, D. The coming of age of de novo protein design. *Nature* **2016**, *537* (7620), 320−327.
(4) Khoury, G. A.; Smadbeck, J.; Kieslich, C. A.; Floudas, C. A. Protein folding and de novo protein design for biotechnological applications. *Trends Biotechnol.* **2014**, *32* (2), 99−109.
(5) Thompson, M. C.; Yeates, T. O.; Rodriguez, J. A. Advances in methods for atomic resolution macromolecular structure determination. *F1000Research* **2020**, *9*, 667.
(6) Robertson, J. C.; Nassar, R.; Liu, C.; Brini, E.; Dill, K. A.; Perez, A. NMR-assisted protein structure prediction with MELDxMD. *Proteins* **2019**, *87* (12), 1333−1340.
(7) Weiner, B. E.; Alexander, N.; Akin, L. R.; Woetzel, N.; Karakas, M.; Meiler, J. BCL:Fold−protein topology determination from limited NMR restraints. *Proteins* **2014**, *82* (4), 587−595.
(8) Vernon, R.; Shen, Y.; Baker, D.; Lange, O. F. Improved chemical shift based fragment selection for CS-Rosetta using Rosetta3 fragment picker. *J. Biomol. NMR* **2013**, *57* (2), 117−127.
(9) Frenz, B.; Walls, A. C.; Egelman, E. H.; Veesler, D.; DiMaio, F. RosettaES: a sampling strategy enabling automated interpretation of difficult cryo-EM maps. *Nat. Methods* **2017**, *14* (8), 797−800.
(10) Lindert, S.; Alexander, N.; Wötzel, N.; Karakaş, M.; Stewart, P. L.; Meiler, J. EM-fold: de novo atomic-detail protein structure determination from medium-resolution density maps. *Structure* **2012**, *20* (3), 464−478.
(11) Artigues, A.; Nadeau, O. W.; Rimmer, M. A.; Villar, M. T.; Du, X.; Fenton, A. W.; Carlson, G. M. Protein Structural Analysis via Mass Spectrometry-Based Proteomics. *Adv. Exp. Med. Biol.* **2016**, *919*, 397−431.
(12) Stiving, A. Q.; VanAernum, Z. L.; Busch, F.; Harvey, S. R.; Sarni, S. H.; Wysocki, V. H. Surface-Induced Dissociation: An Effective Method for Characterization of Protein Quaternary Structure. *Anal. Chem.* **2019**, *91* (1), 190−209.
(13) Konijnenberg, A.; Butterer, A.; Sobott, F. Native ion mobility-mass spectrometry and related methods in structural biology. *Biochim. Biophys. Acta* **2013**, *1834* (6), 1239−1256.
(14) Marklund, E. G.; Degiacomi, M. T.; Robinson, C. V.; Baldwin, A. J.; Benesch, J. L. Collision cross sections for structural proteomics. *Structure* **2015**, *23* (4), 791−799.
(15) Abramson, J.; Adler, J.; Dunger, J.; Evans, R.; Green, T.; Pritzel, A.; Ronneberger, O.; Willmore, L.; Ballard, A. J.; Bambrick, J.; et al. Accurate structure prediction of biomolecular interactions with AlphaFold 3. *Nature* **2024**, *630* (8016), 493−500.
(16) Wohlwend, J.; Corso, G.; Passaro, S.; Reveiz, M.; Leidal, K.; Swiderski, W.; Portnoi, T.; Chinn, I.; Silterra, J.; Jaakkola, T.et al. Boltz-1 Democratizing Biomolecular Interaction Modeling, 2024. DOI: 10.1101/2024.11.19.624167.
(17) Baek, M.; DiMaio, F.; Anishchenko, I.; Dauparas, J.; Ovchinnikov, S.; Lee, G. R.; Wang, J.; Cong, Q.; Kinch, L. N.; Schaeffer, R. D.; et al. Accurate prediction of protein structures and interactions using a three-track neural network. *Science* **2021**, *373* (6557), 871−876.
(18) Agarwal, V.; McShan, A. C. The power and pitfalls of AlphaFold2 for structure prediction beyond rigid globular proteins. *Nat. Chem. Biol.* **2024**, *20* (8), 950−959.
(19) Seffernick, J. T.; Lindert, S. Hybrid methods for combined experimental and computational determination of protein structure. *J. Chem. Phys.* **2020**, *153* (24), No. 240901.
(20) Biehn, S. E.; Lindert, S. Protein Structure Prediction with Mass Spectrometry Data. *Annu. Rev. Phys. Chem.* **2022**, *73*, 1−19.
(21) Leman, J. K.; Weitzner, B. D.; Lewis, S. M.; Adolf-Bryfogle, J.; Alam, N.; Alford, R. F.; Aprahamian, M.; Baker, D.; Barlow, K. A.; Barth, P.; et al. Macromolecular modeling and design in Rosetta: recent methods and frameworks. *Nat. Methods* **2020**, *17* (7), 665−680.
(22) Bonvin, P.; Bonvin, A. Integrative Modelling of Biomolecular Complexes. *J. Mol. Biol.* **2020**, *432* (9), 2861−2881.
(23) Bullock, J. M. A.; Sen, N.; Thalassinos, K.; Topf, M. Modeling Protein Complexes Using Restraints from Crosslinking Mass Spectrometry. *Structure* **2018**, *26*, 1015−1024, DOI: 10.1016/j.str.2018.04.016.
(24) Khakzad, H.; Vermeul, S.; Malmström, L. Quaternary Structure Modeling Through Chemical Cross-Linking Mass Spectrometry: Extending TX-MS Jupyter Reports. *J. Vis. Exp.* **2021**, *176*, No. e60311, DOI: 10.3791/60311.
(25) Aprahamian, M. L.; Chea, E. E.; Jones, L. M.; Lindert, S. Rosetta Protein Structure Prediction from Hydroxyl Radical Protein Footprinting Mass Spectrometry Data. *Anal. Chem.* **2018**, *90* (12), 7721−7729.
(26) Aprahamian, M. L.; Lindert, S. Utility of Covalent Labeling Mass Spectrometry Data in Protein Structure Prediction with Rosetta. *J. Chem. Theory Comput.* **2019**, *15* (5), 3410−3424.
(27) Day, E. H.; Lindert, S. Extracting Residue Solvent Exposure from Covalent Labeling Data with Machine Learning: A Hybrid Approach for Protein Structure Prediction. *J. Am. Soc. Mass Spectrom.* **2025**, *36* (6), 1336−1347.
(28) Biehn, S. E.; Limpikirati, P.; Vachet, R. W.; Lindert, S. Utilization of Hydrophobic Microenvironment Sensitivity in Diethylpyrocarbonate Labeling for Protein Structure Prediction. *Anal. Chem.* **2021**, *93* (23), 8188−8195.
(29) Schmidt, C.; Macpherson, J. A.; Lau, A. M.; Tan, K. W.; Fraternali, F.; Politis, A. Surface Accessibility and Dynamics of Macromolecular Assemblies Probed by Covalent Labeling Mass Spectrometry and Integrative Modeling. *Anal. Chem.* **2017**, *89* (3), 1459−1468.
(30) Bolz, R. M.; Seffernick, J. T.; Drake, Z. C.; Harvey, S. R.; Wysocki, V. H.; Lindert, S. Energy Resolved Mass Spectrometry Data from Surfaced Induced Dissociation Improves Prediction of Protein Complex Structure. *Anal. Chem.* **2025**, *97* (4), 2375−2383.
(31) Seffernick, J. T.; Harvey, S. R.; Wysocki, V. H.; Lindert, S. Predicting Protein Complex Structure from Surface-Induced Dissociation Mass Spectrometry Data. *ACS Cent. Sci.* **2019**, *5* (8), 1330−1341.

(32) Seffernick, J. T.; Canfield, S. M.; Harvey, S. R.; Wysocki, V. H.; Lindert, S. Prediction of Protein Complex Structure Using Surface-Induced Dissociation and Cryo-Electron Microscopy. *Anal. Chem.* **2021**, *93* (21), 7596−7605.
(33) Snyder, D. T.; Harvey, S. R.; Wysocki, V. H. Surface-induced Dissociation Mass Spectrometry as a Structural Biology Tool. *Chem. Rev.* **2022**, *122* (8), 7442−7487.
(34) Sahasrabuddhe, A.; Hsia, Y.; Busch, F.; Sheffler, W.; King, N. P.; Baker, D.; Wysocki, V. H. Confirmation of intersubunit connectivity and topology of designed protein complexes by native MS. *Proc. Natl. Acad. Sci. U.S.A.* **2018**, *115* (6), 1268−1273.
(35) Degiacomi, M. T. On the Effect of Sphere-Overlap on Super Coarse-Grained Models of Protein Assemblies. *J. Am. Soc. Mass Spectrom.* **2019**, *30* (1), 113−117.
(36) Eschweiler, J. D.; Frank, A. T.; Ruotolo, B. T. Coming to Grips with Ambiguity: Ion Mobility-Mass Spectrometry for Protein Quaternary Structure Assignment. *J. Am. Soc. Mass Spectrom.* **2017**, *28* (10), 1991−2000.
(37) Jurneczko, E.; Barran, P. E. How useful is ion mobility mass spectrometry for structural biology? The relationship between protein crystal structures and their collision cross sections in the gas phase. *Analyst* **2011**, *136* (1), 20−28.
(38) McCabe, J. W.; Mallis, C. S.; Kocurek, K. I.; Poltash, M. L.; Shirzadeh, M.; Hebert, M. J.; Fan, L.; Walker, T. E.; Zheng, X.; Jiang, T.; et al. First-Principles Collision Cross Section Measurements of Large Proteins and Protein Complexes. *Anal. Chem.* **2020**, *92* (16), 11155−11163.
(39) Politis, A.; Park, A. Y.; Hall, Z.; Ruotolo, B. T.; Robinson, C. V. Integrative modelling coupled with ion mobility mass spectrometry reveals structural features of the clamp loader in complex with single-stranded DNA binding protein. *J. Mol. Biol.* **2013**, *425* (23), 4790−4801.
(40) Turzo, S. M. B. A.; Seffernick, J. T.; Rolland, A. D.; Donor, M. T.; Heinze, S.; Prell, J. S.; Wysocki, V. H.; Lindert, S. Protein shape sampled by ion mobility mass spectrometry consistently improves protein structure prediction. *Nat. Commun.* **2022**, *13* (1), No. 4377.
(41) Eschweiler, J. D.; Farrugia, M. A.; Dixit, S. M.; Hausinger, R. P.; Ruotolo, B. T. A Structural Model of the Urease Activation Complex Derived from Ion Mobility-Mass Spectrometry and Integrative Modeling. *Structure* **2018**, *26*, 599−606, DOI: 10.1016/j.str.2018.03.001.
(42) Lindert, S.; Staritzbichler, R.; Wötzel, N.; Karakaş, M.; Stewart, P. L.; Meiler, J. EM-fold: De novo folding of alpha-helical proteins guided by intermediate-resolution electron microscopy density maps. *Structure* **2009**, *17* (7), 990−1003.
(43) Lindert, S.; Hofmann, T.; Wötzel, N.; Karakaş, M.; Stewart, P. L.; Meiler, J. Ab initio protein modeling into CryoEM density maps using EM-Fold. *Biopolymers* **2012**, *97* (9), 669−677.
(44) Wang, R.-R.; Song, Y.; Barad, B. A.; Cheng, Y.; Fraser, J. S.; DiMaio, F. Automated structure refinement of macromolecular assemblies from cryo-EM maps using Rosetta. *eLife* **2016**, *5*, No. e17219, DOI: 10.7554/eLife.17219.
(45) Lau, A. M.; Politis, A. Integrative Mass Spectrometry-Based Approaches for Modeling Macromolecular Assemblies. *Methods Mol. Biol.* **2021**, *2247*, 221−241.
(46) Sali, A. From integrative structural biology to cell biology. *J. Biol. Chem.* **2021**, *296*, 100743.
(47) Turzo, S. M. B. A.; Seffernick, J. T.; Lyskov, S.; Lindert, S. Predicting ion mobility collision cross sections using projection approximation with ROSIE-PARCS webserver. *Brief. Bioinf.* **2023**, *24* (5), No. bbad308, DOI: 10.1093/bib/bbad308.
(48) Song, Y.; DiMaio, F.; Wang, R. Y.; Kim, D.; Miles, C.; Brunette, T.; Thompson, J.; Baker, D. High-resolution comparative modeling with RosettaCM. *Structure* **2013**, *21* (10), 1735−1742.
(49) Gront, D.; Kulp, D. W.; Vernon, R. M.; Strauss, C. E.; Baker, D. Generalized fragment picking in Rosetta: design, protocols and applications. *PLoS One* **2011**, *6* (8), No. e23294.
(50) Alford, R. F.; Leaver-Fay, A.; Jeliazkov, J. R.; O'Meara, M. J.; DiMaio, F. P.; Park, H.; Shapovalov, M. V.; Renfrew, P. D.; Mulligan, V. K.; Kappel, K.; et al. The Rosetta All-Atom Energy Function for Macromolecular Modeling and Design. *J. Chem. Theory Comput.* **2017**, *13* (6), 3031−3048.
(51) Zhang, Y.; Skolnick, J. TM-align: a protein structure alignment algorithm based on the TM-score. *Nucleic Acids Res.* **2005**, *33* (7), 2302−2309.
(52) Meng, E. C.; Goddard, T. D.; Pettersen, E. F.; Couch, G. S.; Pearson, Z. J.; Morris, J. H.; Ferrin, T. E. UCSF ChimeraX: Tools for structure building and analysis. *Protein Sci.* **2023**, *32* (11), No. e4792.
(53) Woetzel, N.; Lindert, S.; Stewart, P. L.; Meiler, J. BCL:EM-Fit: rigid body fitting of atomic structures into density maps using geometric hashing and real space refinement. *J. Struct. Biol.* **2011**, *175* (3), 264−276.
(54) Bush, M. F.; Hall, Z.; Giles, K.; Hoyes, J.; Robinson, C. V.; Ruotolo, B. T. Collision Cross Sections of Proteins and Their Complexes: A Calibration Framework and Database for Gas-Phase Structural Biology. *Anal. Chem.* **2010**, *82* (22), 9557−9565.
(55) DiMaio, F.; Tyka, M. D.; Baker, M. L.; Chiu, W.; Baker, D. Refinement of protein structures into low-resolution density maps using rosetta. *J. Mol. Biol.* **2009**, *392* (1), 181−190.
(56) Saldaño, T.; Escobedo, N.; Marchetti, J.; Zea, D. J.; Mac Donagh, J.; Velez Rueda, A. J.; Gonik, E.; García Melani, A.; Novomisky Nechcoff, J.; Salas, M. N.; et al. Impact of protein conformational diversity on AlphaFold predictions. *Bioinformatics* **2022**, *38* (10), 2742−2748.
(57) Chakravarty, D.; Schafer, J. W.; Chen, E. A.; Thole, J. F.; Ronish, L. A.; Lee, M.; Porter, L. L. AlphaFold predictions of fold-switched conformations are driven by structure memorization. *Nat. Commun.* **2024**, *15* (1), No. 7296.
(58) Esser, T. K.; Böhning, J.; Fremdling, P.; Bharat, T.; Gault, J.; Rauschenbach, S. Cryo-EM samples of gas-phase purified protein assemblies using native electrospray ion-beam deposition. *Faraday Discuss.* **2022**, *240* (0), 67−80.
(59) Esser, T. K.; Böhning, J.; Önür, A.; Chinthapalli, D. K.; Eriksson, L.; Grabarics, M.; Fremdling, P.; Konijnenberg, A.; Makarov, A.; Botman, A.; et al. Cryo-EM of soft-landed β-galactosidase: Gas-phase and native structures are remarkably similar. *Sci. Adv.* **2024**, *10* (7), No. eadl4628.
(60) Westphall, M. S.; Lee, K. W.; Hemme, C.; Salome, A. Z.; Mertz, K.; Grant, T.; Coon, J. J. Cryogenic Soft Landing Improves Structural Preservation of Protein Complexes. *Anal. Chem.* **2023**, *95* (40), 15094−15101.
(61) Ohio Supercomputer Center, 1987.

https://doi.org/10.1021/acs.jctc.6c00265
J. Chem. Theory Comput. 2026, 22, 5909−5917